Improved empirical parameterization for projectile fragmentation cross sections

B. Mei*

Institute of Modern Physics, Chinese Academy of Sciences, Lanzhou 730000, China;
Extreme Light Infrastructure Nuclear Physics, "Horia Hulubei" National Institute for Physics and Nuclear Engineering, Strada Reactorului 30, 077125 Bucharest Magurele, Romania;
and GSI-Helmholtzzentrum für Schwerionenforschung GmbH, D-64291 Darmstadt, Germany

(Received 12 January 2017; published 17 March 2017; corrected 30 March 2017)

A new empirical parametrization is developed for calculating the fragment cross sections in projectile fragmentation reactions at high energies (>100 MeV/nucleon). The new parametrization, FRACS, consists of two main parts, i.e., the mass yield and the isobaric distribution, on the basis of previous parametrizations. The formalism for the mass yield is improved to describe the target and the projectile energy dependences observed in measured fragmentation cross sections. The parametrization of the isobaric distribution is also modified to reproduce recent experimental data. Furthermore, an additional term is proposed and first implemented in the FRACS parametrization to account for the evident odd-even staggering effect observed in many experimental cross sections. Comparisons with extensive cross sections measured in various fragmentation reactions reveal that FRACS is in much better agreement with experimental data and can reproduce measured cross sections in most cases within a factor of 1.84, which is a much smaller rms deviation as compared to that of the recent parametrization EPAX3.

DOI: 10.1103/PhysRevC.95.034608

I. INTRODUCTION

Since the pioneering experiments at the Lawrence Berkeley Laboratory [1–3], projectile fragmentation has been widely used to produce and study radioactive beams of exotic nuclei far from stability at present nuclear facilities around the world [4]. For example, a large number of fragmentation reactions at high energies (>100 MeV/nucleon) have been measured at the Fragment Separator (FRS) at GSI [5–15], the A1900 separator at MSU [16–18], and the RIBLL-CSR facility at IMP [19,20] by using a time-of-flight detector [21]. Projectile fragmentation is also one of the most important techniques for future experiments at next generation radioactive beam facilities, e.g., FAIR at GSI [22], FRIB at MSU [23], and HIAF at IMP [24]. Furthermore, fragmentation reactions play an important role in modeling of cosmic-ray propagation in the galaxy and cancer therapy using heavy ions [25,26].

For designing nuclear physics experiments as well as applications in astrophysics and medical therapy, an accurate prediction of fragmentation cross sections is essential. Because the statistical model calculations can be rather time consuming, a fast and accurate empirical parametrization of fragmentation cross sections is very useful for the above applications. Based on previous works by Rudstam [27] and Silberberg and Tsao [28–30], Sümmerer *et al.* proposed a universal empirical parametrization of fragmentation cross sections called EPAX [31]. This original EPAX parametrization was mainly fitted to the measured proton-induced spallation cross sections, due to the lack of experimental data from heavy-ion-induced fragmentation reactions at that time. It was revised in 2000 [32] and 2012 [33] when more heavy-ion-induced fragmentation data became available.

It seems that the latest version of the EPAX parametrization, EPAX3 [33], is in much better agreement with experimental data, especially for very neutron-rich fragments. However, very large discrepancies remain for some neutron-rich fragments. For instance, cross sections of the neutron-rich Tl, Hg, and Au isotopes, produced by ^{208}Pb fragmentation on a ^{nat}Cu target [7] as well as a ^{9}Be target [14], were severely underestimated by EPAX3 [33]. In addition, large discrepancies were observed for the I, Pd, and Rh isotopes, produced by ^{136}Xe fragmentation on a ^{9}Be target [11]; see Ref. [33]. These discrepancies occur because their isotopic distributions were not properly described by EPAX3. Therefore, the accuracy of the EPAX3 parametrization should be improved, in particular for fragments far from stability, where very large discrepancies have been observed.

In the EPAX parametrization, the so-called "limiting fragmentation" was assumed to be valid; see Refs. [31–33] for details. According to this assumption, the cross sections of fragments become independent of the bombarding energy and only depend on the target through a geometrical scaling factor in the high-energy limit of fragmentation reactions, which forms the basis for EPAX. However, recent experimental data measured at energies around 100 MeV/nucleon show a strong target dependence [34,35], especially for nuclei far from stability. In addition, an energy dependence has also been suggested for fragmentation reactions at energies below 200 MeV/nucleon [36], based on recent experimental data. The breakdown of the limiting fragmentation assumption demonstrates that further improvements of the parametrization are required to accurately predict the fragment cross sections, where the observed target dependence, except in the geometrical factor, as well as the energy dependence should be taken into account.

Experimental fragment cross sections (yields) exhibit a pronounced odd-even staggering (OES), which means an

*meibo@impcas.ac.cn

 ©2017 American Physical Society

enhanced production of even-Z nuclides compared with the neighboring odd-Z nuclides. This OES effect has been experimentally observed in many different fragmentation reactions with various projectile-target combinations (see, e.g., Refs. [5,19,20,37–46]). Studies in Refs. [39,41,47] indicate that this OES is related to pairing correlations in nuclear binding (separation) energies. Recent experimental investigations reveal that this OES is mainly due to the OES in particle-emission threshold energies (PETE), where the strong impact of both nuclear pairing and shell structure exists [19,20]. However, this evident OES effect in fragment cross sections is not considered in the EPAX parametrization. As a result, EPAX may underpredict the cross sections of even-Z fragments and overestimate those of odd-Z ones.

To accurately predict the fragment cross sections and remove the large discrepancies between the EPAX predictions and measured cross sections, a new empirical parametrization, called FRACS, is proposed on the basis of EPAX. This new parametrization mainly consists of two parts, namely, the mass distribution and the isobaric distribution, very similar to the EPAX parametrization. In FRACS, an improved mass distribution, where the target dependence as well as the energy dependence are taken into account, is developed by fits to a large set of experimental data from a large variety of fragmentation reactions with different projectile-target combinations at various energies above about 100 MeV/nucleon. Furthermore, the isobaric distribution from EPAX is modified to achieve a much better agreement with the measured data. Last, but not least, a new OES correction term is added in the FRACS parametrization to account for the OES effect observed in many measured cross sections.

In the following, the basic equation of FRACS will be introduced first and then different terms in this equation, including the mass yield, the isobaric distribution, additional corrections for very proton- and neutron-rich fragments, and the OES term will be described separately. After this, predictions by FRACS will be compared with experimental data used in the fitting procedure. Next, predictions by FRACS will also be compared with other experimental data to check the validity of FRACS as well as its parameters. Finally, the overall quality of the new parametrization will be studied.

II. FRAGMENTATION CROSS SECTION FORMULA

A. Basis of parametrization

The analytical formulas for residue cross sections in both spallation and fragmentation reactions were first proposed by Rudstam [27] and later improved by Silberberg and Tsao [28–30] as well as Sümmerer *et al.* [31]. According to their parametrizations, the basic equation for calculating the production cross section of a final fragment with mass number A and nuclear charge Z is

$$\sigma(A,Z) = Y(A)Y(Z_{\rm prob} - Z). \tag{1}$$

The mass yield $Y(A)$ is the sum of all isobaric cross sections with fragment mass A. The isobaric distribution $Y(Z_{\rm prob} - Z)$ represents the distribution of elemental cross sections with a given mass A and its maximum value is reached at the most probable charge, $Z_{\rm prob}$. By using Eq. (1), Sümmerer and Blank developed a modified EPAX parametrization for fragmentation reactions [32], based on heavy-ion-induced reaction data, and it was improved by Sümmerer in a recent work [33].

For heavy-ion-induced fragmentation reactions at high energies, $Y(A)$ can be approximated by an exponential function of mass differences between the projectile and fragments, $(A_p - A)$. In EPAX, the slope of this exponential depends only on the projectile mass but is independent of the target and the bombarding energy [31–33], following the hypothesis of limiting fragmentation. However, this is mainly based on the model and experimental results for proton-induced spallation reactions; see Ref. [31]. Since the slope factor has a significant impact on the prediction of mass yields and thus on the predicted fragment cross sections, the possible dependence on the target and bombarding energy is investigated in this work. Based on recent experimental fragmentation data, a new parametrization function is developed for the slope factor in mass yields. After this, parametrizations for both $Y(A)$ and $Y(Z_{\rm prob} - Z)$ are improved in order to accurately predict the fragmentation cross sections. At last, a new OES term $\Delta_{\rm OES}$ is proposed and the smooth analytical formula [Eq. (1)] should be corrected by this OES term. The corrected cross section is

$$\sigma(A,Z) = Y(A)Y(Z_{\rm prob} - Z)\Delta_{\rm OES}(A,Z). \tag{2}$$

The new parametrization FRACS is based on Eq. (2). In the following, details of different terms used in the FRACS parametrization will be introduced separately.

B. FRACS parametrization

1. Mass yield

According to many previous empirical parametrizations (see, e.g., Refs. [27–33]), the mass yield $Y(A)$ decreases exponentially with increasing $(A_p - A)$, which is also in very good agreement with fragment cross sections measured at high energies. By applying the multiple scattering theory, a simple analytical expression for $Y(A)$ was derived by Abul-Magd, Friedman, and Hüfner [48]:

$$Y(A) = \sigma_R P \exp[-P(A_p - A)], \tag{3}$$

where P is the slope of this exponential and σ_R is the geometrical scaling factor. This equation, which is very similar to mass yield formulas used by Rudstam [27] and by Silberberg and Tsao [28–30], has been adopted in EPAX [31–33] and is also applied in this work.

Recently, many comprehensive data sets of cross sections have been measured for fragmentation reactions with various projectile-target combinations at different energies (see, e.g., Refs. [12,16]). Experimental mass yields can be derived from these complete cross sections. To reproduce these mass yields measured in various reaction systems, a new parametrization of the slope P is developed:

$$\begin{aligned} P = {} & p_1/A_p + p_2/\left(A_t^{1/3}A_p^{1/2}\right) + p_3/(A_t E_p) \\ & + p_4 A_t \log_{10}(E_p/100) + p_5, \end{aligned} \tag{4}$$

where A_p and A_t are the projectile and target mass numbers, respectively, and E_p is the projectile energy in MeV/nucleon. In this expression, the slope P is not only a function of the

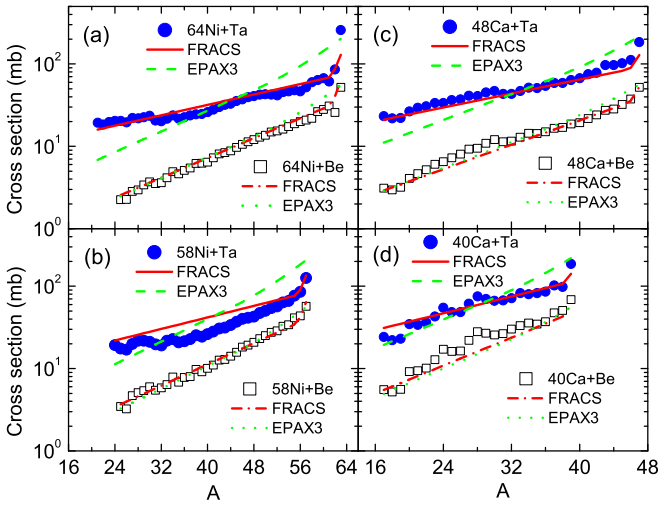

FIG. 1. Mass yields for fragments produced in projectile fragmentation of ^{64,58}Ni and ^{48,40}Ca on ^{9}Be (open squares) and ^{181}Ta (filled circles) targets at 140 MeV/nucleon [16]. Experimental data are compared with predictions by FRACS (full and dash-dotted lines for Ta and Be targets, respectively) as well as EPAX3 (dashed and dotted lines for Ta and Be targets, respectively). For clarity, all Be target data have been scaled by a factor of 0.5. The relative uncertainty of most experimental data is around 10%.

projectile mass A_p but also a function of the target mass A_t and the projectile energy E_p. This new parametrization for P is in very good agreement with experimental data measured in different fragmentation reactions (see below).

Considering the peripheral nature of fragmentation reactions, the geometrical scaling factor in EPAX mainly depends on the sum of the projectile and target radii $(A_p^{1/3} + A_t^{1/3})$ [31–33]. After the inclusion of an energy dependence and a neutron excess dependence, the new scaling factor used in FRACS is parametrized as

$$\sigma_R = s_1\big[A_p^{1/3} + A_t^{1/3} + s_2(A_p - 2Z_p)Z_t/(A_pA_t) + s_3A_pA_t\log_{10}(E_p/100) + s_4\big]\ \text{barn}, \quad (5)$$

where Z_p and Z_t are the projectile and target atomic numbers, respectively, and E_p is the projectile energy in MeV/nucleon.

For fragments far away from the projectile, predictions by Eqs. (3)–(5) are in very good agreement with measured mass yields; see Fig. 1. However, a correction is required to reproduce the rapid increase of the mass yields for fragments very close to the projectile. Therefore, the following correction has been introduced for fragments with $A/A_p > 0.95$:

$$Y'(A) = Y(A)[1 + y_1A_p(x - y_2)^2], \quad (6)$$

where $x = A/A_p$.

Figure 1 illustrates the comparison of measured mass yields for fragmentation of ^{64,58}Ni and ^{48,40}Ca projectiles on ^{9}Be and ^{181}Ta targets at 140 MeV/nucleon [16] with predictions by FRACS [see Eqs. (3)–(6)] and EPAX3. One can clearly see that FRACS can reproduce the slope of mass yields for both heavy Ta and light Be targets, and mass yields predicted by FRACS are in very good agreement with these measured data. EPAX3 also agrees well with the Be target data, despite a small discrepancy for fragments near the projectile. However, EPAX3 cannot reproduce the slope P for almost all Ta target data and thus there are very large discrepancies between the EPAX3 predictions and the Ta target experimental data. Obviously, FRACS is in much better agreement with measured mass yields than EPAX3, especially for the heavy Ta target data.

It should be mentioned that it is hard to describe the mass yields over a large range of A with a simple exponential function of $(A_p - A)$ for fragmentation reactions at lower energies (<100 MeV/nucleon); see, e.g., Refs. [36,49]. Thus, a large deviation may occur when the above equations are applied for fragmentation reactions at energies much lower than 100 MeV/nucleon. Similar to EPAX3, this parametrization is restricted to low-fissility systems, where the projectile mass number should be less than about 210.

2. *Isobaric distribution*

The isobaric (charge) distribution shows Gaussian-like shapes, except for fragments close to the projectile, which are governed by the statistical evaporation from excited prefragments. In this work, the isobaric distribution is based on the EPAX3 parametrization, while some important modifications are introduced to obtain a much better agreement with extensive experimental data. The charge distribution of fragments with a given mass A around the most probable charge Z_{prob} is parametrized according to the following formula [27–33]:

$$Y(Z_{\text{prob}} - Z) = n\exp(-R|Z_{\text{prob}} - Z|^U). \quad (7)$$

The normalization factor $n = \sqrt{R/\pi}$ is applied to normalize the integral of the charge distribution to unity. As shown in Eq. (7), $Y(Z_{\text{prob}} - Z)$ is dominated by three parameters: the width R, the most probable charge Z_{prob}, and the exponent U. Because the charge distribution is asymmetric on the neutron- and proton-rich sides, the parameter U has two different values, U_n and U_p, on the neutron- and proton-rich sides, respectively. In order to reproduce measured fragmentation cross sections, improved parametrizations have been developed for the above parameters, which will be discussed separately in the following.

a. Most probable charge Z_{prob}. According to the parametrization used in EPAX3 [33], the most probable charge Z_{prob} can be expressed as

$$Z_{\text{prob}} = Z_\beta + \Delta + \Delta_m, \quad (8)$$

where the β-stable charge Z_β is approximated by a function of the mass number A

$$Z_\beta = A/(1.98 + 0.0155A^{2/3}). \quad (9)$$

For projectiles near β stability, the sum $(Z_\beta + \Delta)$ defines the so-called evaporation corridor, where the fragments end up after evaporations from excited compound nuclei. This evaporation corridor is similar to the evaporation attractor line proposed in Ref. [50]. The last term Δ_m accounts for the memory effect, which has two different values Δ_m^p and Δ_m^n for projectiles on the proton- and neutron-rich sides, respectively.

In EPAX3, Δ is a linear function of the fragment mass for heavy fragments [33]. Compared to EPAX3, higher-order terms are added in the FRACS parametrization of Δ for heavy fragments with mass $A \geqslant 72$, and thus

$$\begin{aligned} &\text{for } A \geqslant d_6, \quad \Delta = d_1 + d_2 A + d_3 A^2 + d_4 A^3, \\ &\text{for } A < d_6, \quad \Delta = d_5 A^2. \end{aligned} \tag{10}$$

According to experimental data, $Z_{\rm prob}$ becomes close to Z_p for fragments close to the projectile and a correction is needed for Δ. Similar to EPAX3, Δ has to be corrected according to

$$\Delta' = \Delta[1 + d_7(x - d_8)^2], \tag{11}$$

for fragments with $A/A_p > d_8$.

Finally, additional corrections Δ_m^p and Δ_m^n are required for the proton-rich and neutron-rich projectiles, respectively. The same functions have been used as in EPAX3 [33]:

$$\Delta_m^p = (Z_p - Z_{\beta p}) \exp(d_{p1} + d_{p2} x), \tag{12}$$

for proton-rich projectiles with $(Z_p - Z_{\beta p}) > 0$, while

$$\Delta_m^n = (Z_p - Z_{\beta p})(d_{n1} x^2 + d_{n2} x^4), \tag{13}$$

for neutron-rich projectiles with $(Z_p - Z_{\beta p}) \leqslant 0$. The β-stable charge for the projectile $Z_{\beta p}$ can be calculated by Eq. (9).

b. Width parameter R. In EPAX3 [33], the width parameter R has been approximated by a simple exponential function of the fragment mass number A only. To improve the description of recent experimental data, the exponential function is modified in this work:

$$R = R_0 \exp[r_1 A + r_2 A^2 + (r_3 + Z_p - Z_{\beta p})(r_4 + r_5 x)]. \tag{14}$$

Thus, the exponential term in Eq. (14) also depends on the distance of products from the projectile ($x = A/A_p$) as well as the proton or neutron excess of the projectile ($Z_p - Z_{\beta p}$).

According to EPAX3 [33], charge distributions are a bit wider for fragments from neutron-rich projectiles, and thus R_0 has two different values R_0^n and R_0^p for neutron- and proton-rich projectiles, respectively. The same expressions proposed in EPAX3 are adopted in FRACS:

$$R_0^n = r_0 \exp[r_6(Z_p - Z_{\beta p})], \tag{15}$$

for neutron-rich projectiles, and

$$R_0^p = r_0 \exp[r_7(Z_p - Z_{\beta p})], \tag{16}$$

for proton-rich projectiles.

Finally, an additional correction is introduced for fragments close to the projectile considering their much narrower charge distributions. Compared to EPAX3, a modified correction function is obtained in FRACS by fitting to recent experimental data:

$$R' = R \exp\{[r_8 + r_9(Z_p - Z_{\beta p})]\sqrt{A_p}(x - r_{10})^{3.2}\}, \tag{17}$$

which also depends on the proton or neutron excess of the projectile.

c. Exponent parameters U_n and U_p. Two exponent parameters U_n and U_p, which control the falling shapes of charge distributions for fragments on neutron- and proton-rich sides, respectively, are taken as constants in EPAX3. In order to achieve much better predictions for recent experimental data, modified parametrizations are proposed for U_n and U_p,

$$U_n = u_{n1} + u_{n2}(A/A_p) + u_{n3} A_p, \tag{18}$$

$$U_p = u_{p1} + u_{p2} \ln(R), \tag{19}$$

respectively, where U_n depends on the fragment and projectile masses, and U_p depends on the width parameter R.

3. Corrections for very proton- and neutron-rich fragments

In EPAX3 [33], the quasi-Gaussian shape of the charge distribution turns into an exponential decay beyond a certain transition point $Z_{\rm exp}$ for proton-rich fragments. The same correction is adopted in FRACS and the corrected parametrization is

$$\sigma'(A,Z) = \sigma(A, Z_{\rm exp}) 10^{[l_1 + l_2(A/2)^{0.3}](Z_{\rm exp} - Z)}, \tag{20}$$

for fragments with $Z > Z_{\rm exp}$, where the transition point to the exponential slope is calculated by

$$Z_{\rm exp}(A) = Z_{\rm prob} + [l_1 + l_2(A/2)^{0.3}] \ln(10)/(2R). \tag{21}$$

For neutron-rich fragments from neutron-rich projectiles, a so-called "brute-force factor" is required as proposed in EPAX3 [33]. This downscale factor is proposed as follows:

$$F_{\rm bf}^n = 10^{[-b_{n1}|Z_p - Z_{\beta p}|(Z_\beta - Z + Z_p - Z_{\beta p} + b_{n2})^3]}. \tag{22}$$

This factor is applied for neutron-rich fragments where $(Z_\beta - Z) > (Z_p - Z_{\beta p} + b_{n2})$.

The numerical values of various constants used in the above equations, which are determined by fits to extensive cross sections measured in various fragmentation reactions with different projectile-target combinations, are listed in Table I.

4. Nuclear structure factor: Odd-even staggering

Although the above equations can describe well the general smooth tendency of fragmentation cross sections, it is important to consider the odd-even staggering in order to accurately predict these cross sections. Many data sets measured in various fragmentation reactions indicate that fragment cross sections or yields present a strong OES, especially for light fragments ($Z < 40$) close to the drip lines (see, e.g., Refs. [5,19,20,37–46] and references therein). The origin of this OES effect has also been explored in many studies (see, e.g., Refs. [19,20,39,41,42,45,51,52]). According to these studies, the OES seems to be associated with the de-excitation of the prefragments in the late evaporation process, when the fragments become cooling down in order to exhibit the nuclear structure effect, and the angular momentum correlation during the deexcitation process may also contribute to this OES effect. In particular, recent experimental studies in Refs. [19,20] reveal that this OES effect in fragment cross sections (yields) is dominated by the OES in the particle-emission threshold energies (PETE), where all particle decays cease and the final fragments are formed in the evaporation process. These observations are in good agreement with theoretical models of Campi and Hüfner [53] and Hüfner *et al.* [54]. The PETE value ($S_{\rm pete}$) is determined from the smallest value of either the proton separation energy (S_p) or the neutron separation

TABLE I. Constants used in the new parametrization FRACS.

Parameter	Constant	Value
Mass yield slope P	p_1	2.0
	p_2	0.60
	p_3	15.0
	p_4	5.0×10^{-5}
	p_5	−0.01
Scaling factor σ_R	s_1	0.272
	s_2	−8.0
	s_3	4.00×10^{-5}
	s_4	−1.60
Mass yield correction	y_1	10.0
	y_2	0.95
$Z_{\rm prob}$ shift Δ	d_1	−1.40
	d_2	0.03447
	d_3	3.5×10^{-5}
	d_4	-1.5×10^{-7}
	d_5	2.1353×10^{-4}
	d_6	72
	d_7	−24
	d_8	0.8
p-rich memory effect Δ_m^p	d_{p1}	−10.25
	d_{p2}	10.25
n-rich memory effect Δ_m^n	d_{n1}	0.4
	d_{n2}	0.6
Width R	r_0	2.78
	r_1	−0.015
	r_2	3.2×10^{-5}
	r_3	−1.5
	r_4	−0.12
	r_5	0.2041
	r_6	0.0412
	r_7	0.124
	r_8	45.5
	r_9	−11
	r_{10}	0.855
n-rich slope U_n	u_{n1}	1.26
	u_{n2}	0.6
	u_{n3}	-6.0×10^{-4}
p-rich slope U_p	u_{p1}	2.1
	u_{p2}	−0.16
n-rich brute-force factor	b_{n1}	2.3×10^{-3}
	b_{n2}	2.4
p-rich transition point	l_1	1.2
	l_2	0.647

energy (S_n) of one particular fragment, which contains nuclear structure properties, e.g., nucleon-nucleon pairing and shell effects [19,20]. The emission of α particles is not considered in the determination of the PETE value for the light fragments, where a strong OES in fragment cross sections has been observed. This is supported by the good agreement with experimental data (see below). According to the most recent investigations in Ref. [20], the magnitude of this OES in fragment cross sections is very close to that in PETE when the Coulomb barrier is added to S_p. Similar conclusions are obtained for spallation reactions in Ref. [55]. Based on the above experimental and theoretical studies, the magnitude of OES in fragment cross sections ($D_{\rm CS}$) can be approximated by that in the PETE values ($D_{\rm PETE}$), namely,

$$D_{\rm CS}(A,Z) \approx D_{\rm PETE}(A,Z). \tag{23}$$

$D_{\rm PETE}(A,Z)$ for one particular fragment with an isospin value $T_z = (N-Z)/2$ can be calculated from PETE values of four neighboring fragments along a constant T_z chain, using the following third-order difference formula [19,20]:

$$D_{\rm PETE}(Z) = \tfrac{1}{8}(-1)^{Z+1}\{\ln S_{\rm pete}(Z+3) - \ln S_{\rm pete}(Z) - 3[\ln S_{\rm pete}(Z+2) - \ln S_{\rm pete}(Z+1)]\}. \tag{24}$$

By using this formula, one can also calculate $D_{\rm PETE}(A,Z)$ from PETE values of four neighboring fragments with a constant A value. In general, $D_{\rm CS}(A,Z)$ can be approximated by $D_{\rm PETE}(A,Z)$ values calculated by both methods, while the variation of $S_{\rm pete}$ is much slower for fragments along a constant T_z chain and this chain is far longer than the isobaric (constant A) chain. Thus, it is more suitable to derive $D_{\rm PETE}(A,Z)$ along a constant T_z chain, which is also in very good agreement with $D_{\rm CS}(A,Z)$ measured in fragment cross sections (see below).

The magnitude of OES in fragment cross sections can also be calculated by Eq. (24), where the PETE values should be replaced by cross sections (yields) of four neighboring fragments along a constant T_z chain (see, e.g., Refs. [19,20,56,57]). The derived magnitude value $D_{\rm CS}$ means that the natural logarithms of cross sections of even-Z fragments are larger than the smooth part by an amount $D_{\rm CS}$ and those of odd-Z fragments are less than the smooth part by $D_{\rm CS}$ [56,57]. Supposing that $\sigma_{\rm smooth}(A,Z)$ is the smooth part of the cross section without OES, one can get the following equation:

$$\ln\sigma(A,Z) = \ln\sigma_{\rm smooth}(A,Z) + (-1)^Z D_{\rm CS}(A,Z), \tag{25}$$

and thus the cross section corrected for the OES effect is written as

$$\sigma(A,Z) = \sigma_{\rm smooth}(A,Z)\exp[(-1)^Z D_{\rm CS}(A,Z)], \tag{26}$$

where $D_{\rm CS}(A,Z)$ is the magnitude of OES for the cross section of this particular fragment with mass number A and atomic number Z. It is obvious that the OES term $\Delta_{\rm OES}$ in Eq. (2) is

$$\Delta_{\rm OES}(A,Z) = \exp[(-1)^Z D_{\rm CS}(A,Z)]. \tag{27}$$

In this work, $D_{\rm CS}(A,Z)$ is approximated by $D_{\rm PETE}(A,Z)$ [see Eq. (23)], which is supported by good agreement with experimental data. Using Eq. (24), one can calculate $D_{\rm PETE}(A,Z)$ for fragments along a constant T_z chain. As described above, $S_{\rm pete}(A,Z)$ is the smallest value of either $(S_p + V_{\rm c})$ or S_n of one particular fragment, when the Coulomb barrier $V_{\rm c}$ is taken into account. Separation energies (S_p and S_n) are obtained from the latest Atomic Mass Evaluation AME'12 [58]. In the cases where separation energies are unavailable in the AME'12, they are determined via the finite-range droplet model (FRDM) [59]. The Coulomb barrier $V_{\rm c}$ can be calculated by using a simple theoretical model [20,60,61]:

$$V_{\rm c}(A,Z) = \frac{1.44(Z-1)}{1.22[(A-1)^{1/3}+1]+6}\ {\rm MeV}, \tag{28}$$

where A and Z are the mass and atomic numbers of this particular fragment, respectively.

Due to the increasing contribution of the smooth Coulomb barrier and the competition between particle evaporation and γ-ray emission, fragment cross sections are almost smooth and thus $D_{CS}(A,Z) = 0$ is assumed for heavy fragments with $A > 150$. It should be emphasized that there are not adjustable parameters in this analytical parametrization of the OES in fragment cross sections, except for the theoretical formula of the Coulomb barrier from Refs. [20,60,61].

Both the smooth distribution and the evident OES effect are now included in the new parametrization FRACS, while the latter is not considered in the previous EPAX parametrizations [31–33]. In the following both FRACS and EPAX3 will be compared with extensive experimental data measured in different fragmentation reactions with a large variety of projectile and target combinations in order to check the predictive power of two parametrizations.

III. COMPARISONS WITH EXPERIMENTAL DATA AND EPAX3

Over the past decades, many comprehensive data sets of fragmentation cross sections have been measured in various reactions with different projectile-target combinations mainly at GSI and MSU. For instance, very complete cross sections of fragments from the fragmentation of ^{64,58}Ni and ^{48,40}Ca projectiles on the light ^{9}Be and the heavy ^{181}Ta targets at 140 MeV/nucleon have been accurately measured at MSU [16]. Additionally, measurements of very comprehensive cross sections for fragments from the fragmentation of ^{124,136}Xe on a ^{208}Pb target at 1 GeV/nucleon have been performed at GSI [12]. These comprehensive experimental data with small uncertainties, where both the mass yields and isobaric distributions are available over a wide mass range, are very useful for the determination of FRACS parameters in the fitting procedure. The FRACS parameters listed in Table I have been obtained by comparisons with these comprehensive experimental data.

However, in most cases, the experimental data are incomplete and only very limited mass yields as well as isobaric distributions have been measured. These incomplete experimental data measured in a large variety of fragmentation reactions can be applied to validate the FRACS parametrization as well as the determined parameters of FRACS.

The extensive comparisons between predictions by FRACS as well as EPAX3 and experimental data measured in various reaction systems will be discussed in the following subsections. The overall quality of FRACS and EPAX3 parametrizations will also be investigated by using different methods.

A. Comparisons with experimental data used in the fitting procedure and EPAX3

The complete fragment cross sections measured from the fragmentation of ^{64,58}Ni and ^{48,40}Ca projectiles on both ^{9}Be and ^{181}Ta targets at 140 MeV/nucleon [16] have been used to determine the FRACS parameters. As an example, Fig. 2 illustrates a sample of measured data from the proton-rich projectile ^{58}Ni fragmentation on the ^{181}Ta target and the predictions by the FRACS and EPAX3 parametrizations. The predictions by the FRACS parametrization are in very good agreement with these measured cross sections, while EPAX3 overestimates cross sections of proton-rich fragments close to the projectile ($Z \sim 27$) and underpredicts cross sections of light neutron-rich fragments with $Z = 12$ and 11.

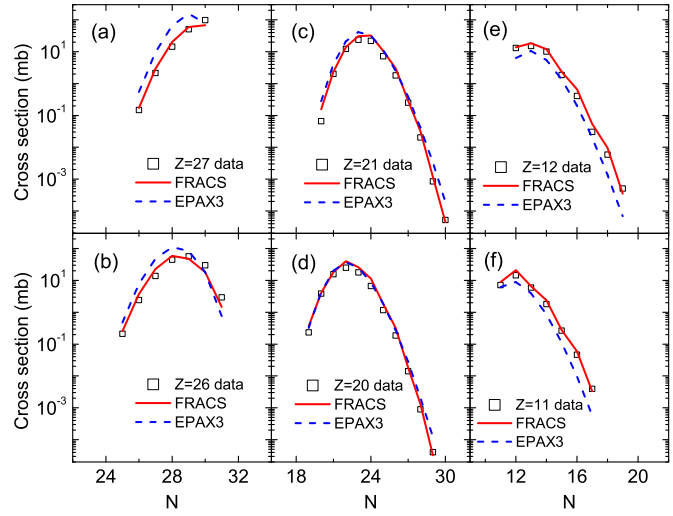

FIG. 2. Sample of experimental isotopic distributions of fragments produced in projectile fragmentation of ^{58}Ni on ^{181}Ta targets at 140 MeV/nucleon [16]. Experimental data (open squares) are compared with predictions by FRACS (full lines) and EPAX3 (dashed lines). The relative uncertainty of most experimental cross section is less than 10%.

In Fig. 3, the fragmentation cross sections for fragments from the neutron-rich projectile ^{64}Ni on the ^{181}Ta target measured by Mocko *et al.* [16] are compared with the predictions by FRACS as well as EPAX3. Predictions by the FRACS parametrization are in much better agreement with the experimental cross sections. However, the EPAX3 parametrization overestimates cross sections of heavier fragments (i.e., $Z = 27$ and 26) near the peak positions and underpredicts those of light fragments with Z from 16 to 12, in particular for very neutron-rich ones.

For the heavy proton-rich projectile, one can compare the experimental cross sections of fragments produced in ^{124}Xe + ^{208}Pb at 1 GeV/nucleon [12] with those predicted by the FRACS and EPAX3 parametrizations, as shown in Fig. 4. EPAX3 overestimates cross sections of very neutron-rich fragments with Z from 49 to 46 and underpredicts those of light neutron-rich fragments with Z from 30 to 27. Although FRACS slightly underpredicts cross sections of some heavy fragments near the peak positions, predictions by FRACS are in good agreement with the experimental data.

For the heavy neutron-rich projectile, Fig. 5 presents the comparison between the fragmentation cross sections measured for ^{136}Xe + ^{208}Pb at 1 GeV/nucleon [12] and those predicted by FRACS as well as EPAX3. Cross sections

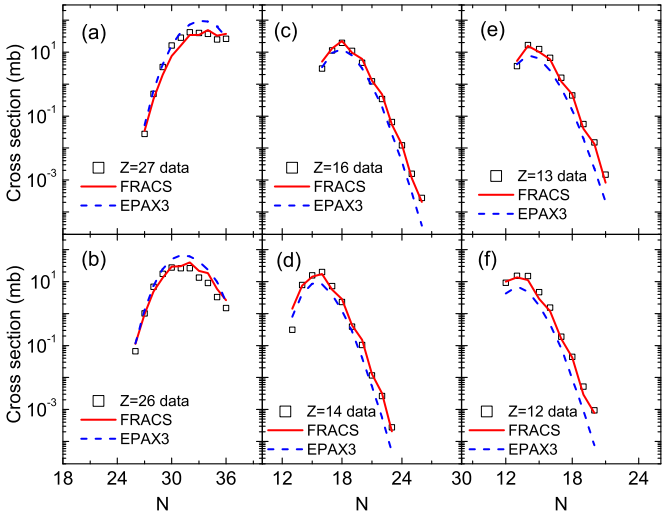

FIG. 3. Sample of experimental isotopic distributions of fragments produced in projectile fragmentation of ^{64}Ni on ^{181}Ta targets at 140 MeV/nucleon [16]. Experimental data (open squares) are compared with predictions by FRACS (full lines) and EPAX3 (dashed lines). The relative uncertainty of experimental cross section is around 10%.

predicted by FRACS are in better agreement with experimental data, while EPAX3 underpredicts cross sections of the proton-rich fragments close to the projectile, especially for the very proton-rich ones, as well as those of the light neutron-rich fragments with $Z \sim 30$.

Experimental fragmentation cross sections show an evident OES effect, which becomes very clear for fragments along a constant T_z chain, as shown in Fig. 6. These cross sections along a constant T_z chain measured in the fragmentation of

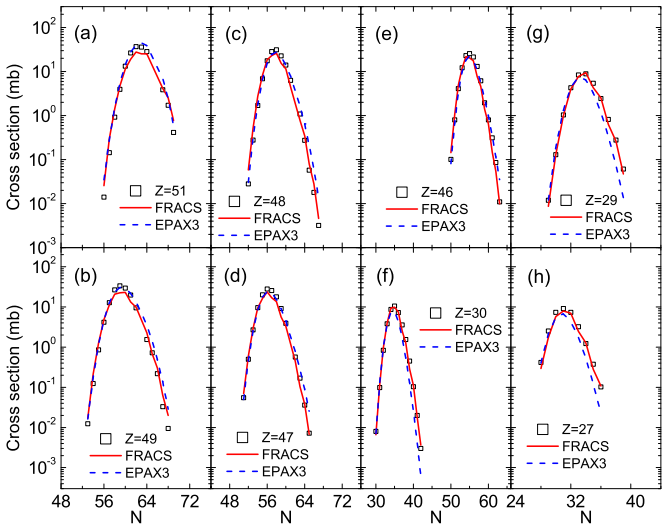

FIG. 4. Sample of experimental isotopic distributions of fragments produced in projectile fragmentation of ^{124}Xe on ^{208}Pb targets at 1 GeV/nucleon [12]. Experimental data (open squares) are compared with predictions by FRACS (full lines) and EPAX3 (dashed lines). The relative uncertainty of experimental data is about 10%.

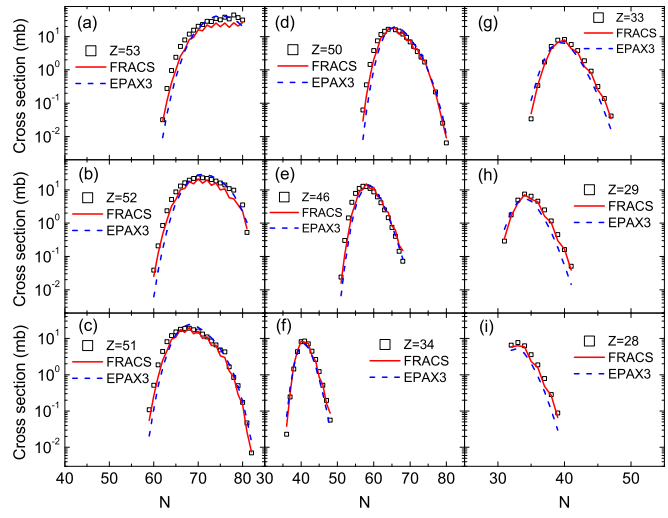

FIG. 5. Sample of experimental isotopic distributions of fragments produced in projectile fragmentation of ^{136}Xe on ^{208}Pb targets at 1 GeV/nucleon [12]. Experimental data (open squares) are compared with predictions by FRACS (full lines) and EPAX3 (dashed lines). The relative uncertainty of most measured cross section is about 10%.

^{58}Ni on ^{181}Ta targets at 140 MeV/nucleon (filled squares) [16] and ^{9}Be targets at 650 MeV/nucleon (open squares) [5] are compared with predictions by FRACS and EPAX3 in Fig. 6. It is obvious that the FRACS predictions agree

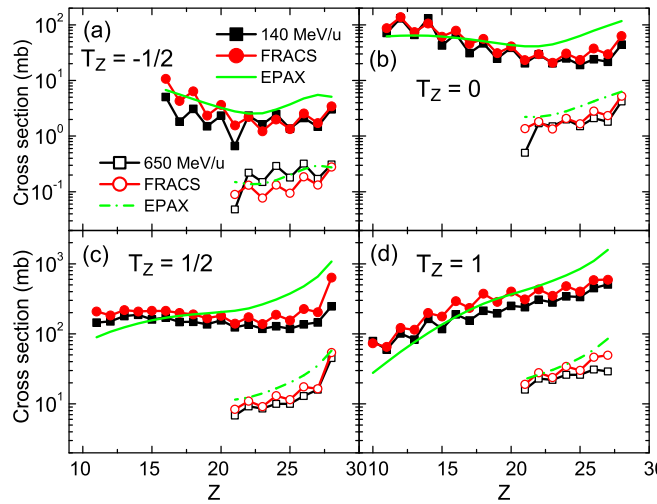

FIG. 6. Experimental cross sections of fragments along a constant T_z chain from $T_z = -1/2$ to $T_z = +1$, produced in the projectile fragmentation of ^{58}Ni on ^{181}Ta targets at 140 MeV/nucleon [16] (filled squares joined by full lines) and ^{9}Be targets at 650 MeV/nucleon [5] (open squares joined by full lines). Experimental data are compared with predictions by FRACS (filled and open circles joined by full lines at 140 and 650 MeV/nucleon, respectively) and EPAX3 (full and dash-dotted green lines at 140 and 650 MeV/nucleon, respectively). For clarity, the data at 140 MeV/nucleon have been scaled by a factor of 10. The relative uncertainty of measured data at 140 MeV/nucleon is about 10%, while it is around 20-30% for most experimental data at 650 MeV/nucleon.

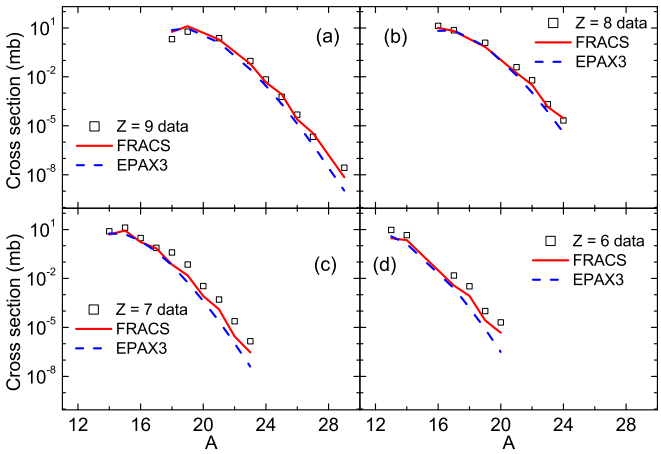

FIG. 7. Measured isotopic distributions of fragments produced in projectile fragmentation of ^{40}Ar on a ^{9}Be target at 1 GeV/nucleon [8]. Experimental data (open squares) are compared with predictions by FRACS (full lines) and EPAX3 (dashed lines). The relative uncertainty of measured cross section is about 30%.

very well with the experimental data at two energies and can reproduce the OES observed in fragmentation cross sections. However, this evident OES effect is not taken into account in EPAX3 and there are very large discrepancies between the EPAX3 predictions and the measured cross sections; see Fig. 6. According to these comparisons, the OES effect is very evident in the fragmentation cross sections and fragmentation models should take this OES effect into account in order to accurately predict fragmentation cross sections.

B. Comparisons with other experimental data and EPAX3

In order to check the validity of the FRACS parametrization as well as its parameters, one can also compare the FRACS predictions with other experimental data, where only limited mass yields and incomplete isobaric distributions have been measured. Additionally, these experimental data are compared with predictions by the recent parametrization EPAX3 [33].

For fragments produced in the fragmentation of the light neutron-rich projectile ^{40}Ar on the ^{9}Be target at 1 GeV/nucleon, Fig. 7 shows the comparison between the experimental cross sections [8] and those predicted by FRACS as well as EPAX3. The experimental cross sections, in particular for very neutron-rich fragments, are significantly underpredicted by EPAX3 by up to two orders of magnitude. Compared to EPAX3, the FRACS predictions are in better agreement with the measured cross sections, despite smaller deviations for some neutron-rich fragments.

Figure 8 presents the experimental cross sections measured from the fragmentation of ^{112}Sn on two different targets, namely, ^{112}Sn [13] and ^{9}Be [9], in comparison with predictions by FRACS as well as EPAX3. The comparison indicates that predictions by both FRACS and EPAX3 are in very good agreement with measured cross sections from the fragmentation of ^{112}Sn on the ^{9}Be target. Predictions by FRACS also agree excellently with the data measured with the ^{112}Sn target,

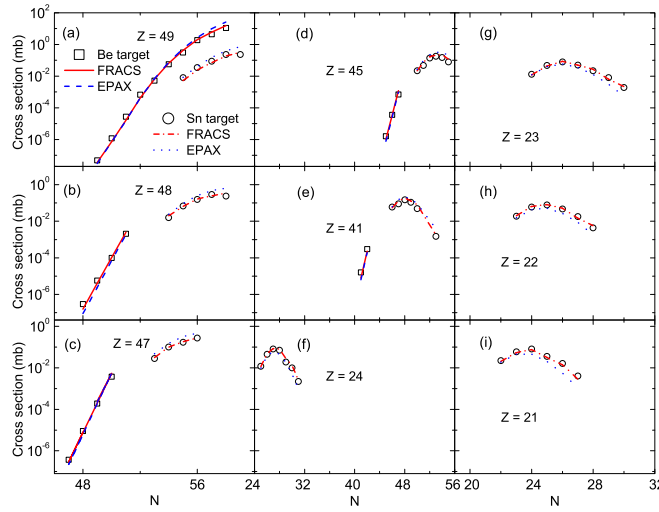

FIG. 8. Experimental isotopic distributions of fragments produced in projectile fragmentation of ^{112}Sn on ^{112}Sn [13] (open circles) and ^{9}Be [9] (open squares) targets at 1 GeV/nucleon. Experimental data are compared with predictions by FRACS (full and dash-dotted lines for Be and Sn targets, respectively) and EPAX3 (dashed and dotted lines for Be and Sn targets, respectively). For clarity, the data from reactions on the ^{112}Sn target have been scaled by a factor of 0.01. The relative uncertainty of ^{112}Sn target experimental data is about 20%, while it is around 40% for Be target experimental data.

while EPAX3 overestimates these experimental data for the most fragments close to the projectile and underpredicts these data for light fragments, especially for the very neutron-rich ones.

As an example for neutron-rich fragments from the medium-mass neutron-rich projectile, Fig. 9 compares the measured fragmentation cross sections from ^{136}Xe + ^{9}Be at

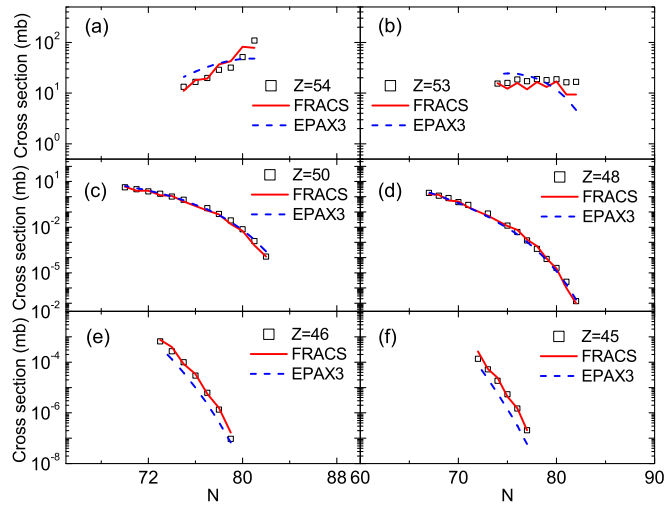

FIG. 9. Measured isotopic distributions of fragments produced in projectile fragmentation of ^{136}Xe on a ^{9}Be target at 1 GeV/nucleon [11]. Experimental data (open squares) are compared with predictions by FRACS (full lines) and EPAX3 (dashed lines). The relative uncertainty of measured data is around 10%.

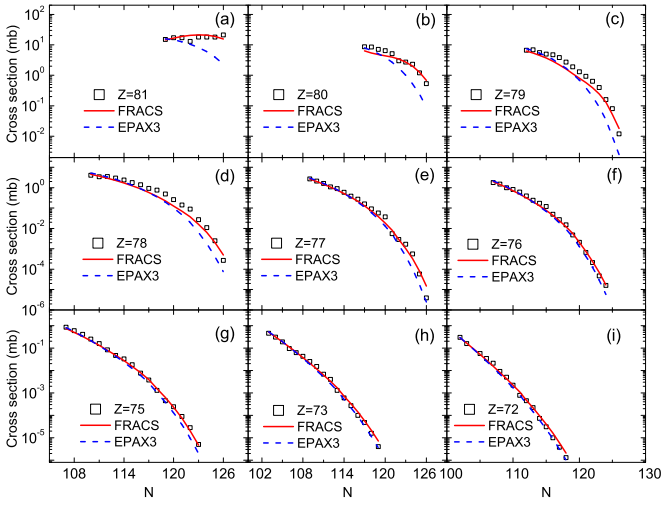

FIG. 10. Experimental isotopic distributions of fragments produced in projectile fragmentation of ^{208}Pb on a ^{9}Be target at 1 GeV/nucleon [14]. Experimental data (open squares) are compared with predictions by FRACS (full lines) and EPAX3 (dashed lines). The relative uncertainty of measured cross section is about 20%.

1 GeV/nucleon [11] with those predicted by FRACS and EPAX3. Cross sections predicted by FRACS are in very good agreement with experimental data, while EPAX3 cannot reproduce the isotopic distributions for fragments with $Z = 54$ and 53. In addition, EPAX3 underpredicts almost all measured cross sections of isotopes with $Z = 45$ and 46, as pointed out in Ref. [33].

One can test the predictive power of FRACS as well as EPAX3 for fragments from heavier projectiles by comparing the predictions by them with measured cross sections of neutron-rich fragments from ^{208}Pb + ^{9}Be at 1 GeV/nucleon [14] (see Fig. 10). It is obvious that FRACS can reproduce the change of the shape of the isotopic distribution from close to the projectile to lighter elements and thus cross sections predicted by FRACS agree well with experimental data. However, EPAX3 fails to reproduce the flat isotopic distribution for $Z = 81$ and significantly underpredicts the cross sections of very neutron-rich fragments with Z from 81 to 78.

The above comparisons between predictions by FRACS as well as EPAX3 and measured data for fragments from various projectile and target combinations, especially for neutron-rich fragments from light, medium-mass, and heavy projectiles, support that FRACS is in much better agreement with experimental data than EPAX3. Additionally, FRACS can reproduce well the shape of the isotopic distribution, while there is a large discrepancy between the isotopic distribution predicted by EPAX3 and the measured one for fragments close to the medium-mass projectile ^{136}Xe and the heavy projectile ^{208}Pb, as shown in Figs. 9 and 10, respectively. After the above important improvements in FRACS, a remarkably better agreement is reached, while small discrepancies remain for some cross sections predicted by FRACS [see, e.g., panel (b) of Fig. 1, panel (a) of Fig. 5, panel (c) of Fig. 7, and panels (c) and (d) of Fig. 10], which will be improved in future works.

C. Overall quality of FRACS and EPAX3

The validity of the empirical parametrizations compared to the experiential data can be visualized by the logarithm of the ratios between the theoretical cross sections predicted by FRACS as well as EPAX3 and the experimental data. Figure 11 illustrates typical examples of the logarithms of these ratios for fragments produced in different fragmentation reactions with a large variety of projectile and target combinations. Obviously, the logarithmic values of the ratios between FRACS and experimental data (red stars) are centered around zero and are much less dispersed than that from EPAX3 (blue circles). For FRACS, more than 90% of these $\log_{10}(\sigma_{\rm th}/\sigma_{\rm exp})$ values are distributed between -0.5 and 0.5. But, for EPAX3, in many cases, these logarithmic values are far larger than 0.5 or smaller than -0.5; see, e.g., data points (blue circles) for fragments produced in ^{40}Ar + ^{9}Be [panel (a)], ^{124}Xe + ^{208}Pb [panel (h)], and ^{136}Xe + ^{208}Pb [panel (j)]. It can be seen that predictions by FRACS are in much better agreement with the experimental data measured in various reaction systems as compared to EPAX3.

To further probe the validity range and the precision of FRACS and EPAX3, the predictions by two parametrizations are compared to more experimental data (about 3700 cross sections measured in various fragmentation reactions [5,7–16]) in Fig. 12, which shows the ratios of theoretical predictions by FRACS as well as EPAX3 to measured cross sections. For FRACS, 95% of the ratio values ($\sigma_{\rm FRACS}/\sigma_{\rm exp}$) are distributed from about 0.28 to 3.5; see squares between two dashed green lines in Fig. 12, corresponding to the range of 2σ. However, for EPAX3, this 2σ range is between roughly 0.17 and 5.8, which is much wider than that of FRACS. As shown in Fig. 12, the ratio value for EPAX3 varies from about 0.01 to 100 and is below 1 for most heavy fragments around $A = 200$. The above comparisons demonstrate that experimental data are much better reproduced by FRACS as compared to EPAX3.

The overall quality of the empirical parametrizations can also be quantitatively evaluated by the rms deviation factor defined via the following equation [62,63]:

$$f_{\rm rms} = \exp\left[\frac{1}{N}\sum_{i=1}^{N}\left(\ln\frac{\sigma_{\rm th}^{i}}{\sigma_{\rm exp}^{i}}\right)^{2}\right]^{1/2}, \qquad (29)$$

where N is the number of measured cross sections (about 3700). According to Eq. (29), the fragmentation cross sections are predicted by FRACS within a factor of 1.84 ($f_{\rm rms} = 1.84$), which is much smaller than the value of 2.35 for EPAX3. Compared to the recent parametrization EPAX3, the new parametrization FRACS therefore gives much better predictions for fragmentation cross sections.

According to the above studies using different methods, it is obvious that FRACS can provide a more reliable prediction for fragmentation cross sections and agrees well with experimental data in most cases within a factor of 1.84. The much better agreement between FRACS and measured cross sections suggests that FRACS is particularly suitable for a fast, accurate, and reliable estimate of fragmentation cross sections.

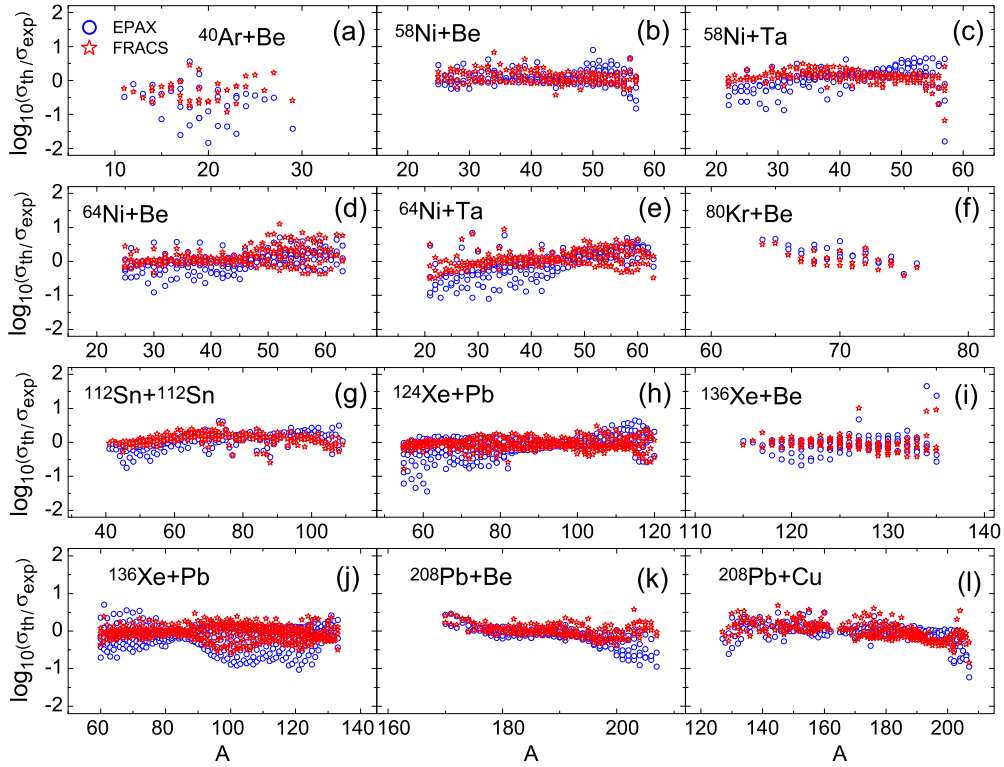

FIG. 11. Logarithm of ratios between predictions of FRACS (open stars) as well as EPAX3 (open circles) and experimental cross sections measured in different reaction systems [7,8,10–14,16].

IV. SUMMARY

A new empirical parametrization, called FRACS, is proposed for accurately predicting fragment cross sections in various fragmentation reactions at energies higher than about 100 MeV/nucleon. The smooth formula of this parametrization consists of the mass yield and the isobaric distribution, based on the previous parametrization EPAX. Suitable modifications are introduced for both the mass yield and the isobaric distribution to reproduce recent experimental data measured in fragmentation reactions with different projectile-target combinations at various energies. Both the target and the projectile energy dependences are taken into account in the FRACS parametrization. In addition, an odd-even staggering term, which was not considered in EPAX, is proposed and now included in FRACS.

Parameters used in FRACS have been optimized by comparing with comprehensive experimental data measured in different fragmentation reactions with a large variety of projectile and target combinations. Furthermore, the predictions by FRACS are also compared with many other experimental data, which are not used in the fitting procedure, in order to check the validity of the FRACS parametrization as well as its parameters. Quantitative investigations by using different methods demonstrate that FRACS can provide a more reliable prediction for fragmentation cross sections and agrees well with experimental data in most cases within a factor of 1.84, which is a much better agreement compared to the recent EPAX3 parametrization. The much better predictive power of FRACS makes it a more reliable model for designing nuclear physics experiments and applications in astrophysics and medical therapy.

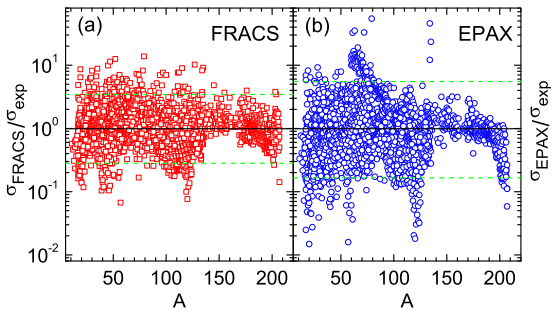

FIG. 12. Ratio of predicted cross sections by FRACS (open squares) and EPAX3 (open circles) to extensive experimental data [5,7–16]. 95% data points are distributed between two dashed green lines in each figure, corresponding to the range of 2σ.

ACKNOWLEDGMENTS

This research was supported by the Extreme Light Infrastructure Nuclear Physics (ELI-NP) Phase II, a project cofinanced by the Romanian Government and the European Union through the European Regional Development Fund, Competitiveness Operational Programme (1/07.07.2016, COP, ID 1334).

[1] M. Buenerd *et al.*, Phys. Rev. Lett. **37**, 1191 (1976).
[2] Y. P. Viyogi *et al.*, Phys. Rev. Lett. **42**, 33 (1979).
[3] G. D. Westfall *et al.*, Phys. Rev. Lett. **43**, 1859 (1979).
[4] D. J. Morrissey and B. M. Sherrill, Philos. Trans. R. Soc. London A **356**, 1985 (1998).
[5] B. Blank *et al.*, Phys. Rev. C **50**, 2398 (1994).
[6] M. Weber *et al.*, Nucl. Phys. A **578**, 659 (1994).
[7] M. de Jong *et al.*, Nucl. Phys. A **628**, 479 (1998).
[8] A. Ozawa *et al.*, Nucl. Phys. A **673**, 411 (2000).
[9] A. Stolz *et al.*, Phys. Rev. C **65**, 064603 (2002).
[10] T. Yamaguchi *et al.*, Phys. Rev. C **74**, 044608 (2006).
[11] J. Benlliure *et al.*, Phys. Rev. C **78**, 054605 (2008).
[12] D. Henzlova *et al.*, Phys. Rev. C **78**, 044616 (2008).
[13] V. Föhr *et al.*, Phys. Rev. C **84**, 054605 (2011).
[14] T. Kurtukian-Nieto *et al.*, Phys. Rev. C **89**, 024616 (2014).
[15] J. Alcántara-Núñez *et al.*, Phys. Rev. C **92**, 024607 (2015).
[16] M. Mocko *et al.*, Phys. Rev. C **74**, 054612 (2006).
[17] O. B. Tarasov *et al.*, Phys. Rev. Lett. **102**, 142501 (2009).
[18] O. B. Tarasov *et al.*, Phys. Rev. C **87**, 054612 (2013).
[19] B. Mei *et al.*, Phys. Rev. C **89**, 054612 (2014).
[20] B. Mei *et al.*, Phys. Rev. C **94**, 044615 (2016).
[21] B. Mei *et al.*, Nucl. Instrum. Methods A **624**, 109 (2010).
[22] T. Nilsson, Eur. Phys. J. Spec. Top. **156**, 1 (2008).
[23] T. Baumann *et al.*, Nucl. Instrum. Methods B **376**, 33 (2016).
[24] J. C. Yang *et al.*, Nucl. Instrum. Methods B **317**, 263 (2013).
[25] L. Sihver, C. H. Tsao, R. Silberberg, T. Kanai, and A. F. Barghouty, Phys. Rev. C **47**, 1225 (1993).
[26] L. Sihver, M. Lantz, and A. Kohama, Phys. Rev. C **89**, 067602 (2014).
[27] G. Rudstam, Z. Naturforsch. **21a**, 1027 (1966).
[28] R. Silberberg and C. H. Tsao, Astrophys. J. Suppl. Ser. **25**, 315 (1973).
[29] R. Silberberg and C. H. Tsao, Astrophys. J. Suppl. Ser. **25**, 335 (1973).
[30] R. Silberberg and C. H. Tsao, Phys. Rep. **191**, 351 (1990).
[31] K. Sümmerer, W. Brüchle, D. J. Morrissey, M. Schädel, B. Szweryn, and Yang Weifan, Phys. Rev. C **42**, 2546 (1990).
[32] K. Sümmerer and B. Blank, Phys. Rev. C **61**, 034607 (2000).
[33] K. Sümmerer, Phys. Rev. C **86**, 014601 (2012).
[34] M. Notani *et al.*, Phys. Rev. C **76**, 044605 (2007).
[35] E. Kwan, D. J. Morrissey, D. A. Davies, M. Steiner, C. S. Sumithrarachchi, and L. Weissman, Phys. Rev. C **86**, 014612 (2012).
[36] X. H. Zhang, Nucl. Phys. A **915**, 59 (2013).
[37] C. Zeitlin *et al.*, Phys. Rev. C **56**, 388 (1997).
[38] E. Geraci *et al.*, Nucl. Phys. A **732**, 173 (2004).
[39] M. V. Ricciardi *et al.*, Nucl. Phys. A **733**, 299 (2004).
[40] C. Zeitlin *et al.*, Phys. Rev. C **77**, 034605 (2008).
[41] M. V. Ricciardi, K. H. Schmidt, and A. Kelić-Heil, arXiv:1007.0386.
[42] M. D'Agostino *et al.*, Nucl. Phys. A **861**, 47 (2011).
[43] G. Casini *et al.*, Phys. Rev. C **86**, 011602(R) (2012).
[44] K. Hagino and H. Sagawa, Phys. Rev. C **85**, 037604 (2012).
[45] M. D'Agostino *et al.*, Nucl. Phys. A **875**, 139 (2012).
[46] J. R. Winkelbauer, S. R. Souza, and M. B. Tsang, Phys. Rev. C **88**, 044613 (2013).
[47] J. J. Gaimard and K. H. Schmidt, Nucl. Phys. A **531**, 709 (1991).
[48] A. Y. Abul-Magd, W. A. Friedman, and J. Hüfner, Phys. Rev. C **34**, 113 (1986).
[49] G. A. Souliotis *et al.*, Phys. Lett. B **543**, 163 (2002).
[50] R. J. Charity, Phys. Rev. C **58**, 1073 (1998).
[51] M. V. Ricciardi *et al.*, Nucl. Phys. A **749**, 122 (2005).
[52] N. L. Calleya, S. R. Souza, B. V. Carlson, R. Donangelo, W. G. Lynch, M. B. Tsang, and J. R. Winkelbauer, Phys. Rev. C **90**, 054616 (2014).
[53] X. Campi and J. Hüfner, Phys. Rev. C **24**, 2199 (1981).
[54] J. Hüfner, C. Sander, and G. Wolschin, Phys. Lett. B **73**, 289 (1978).
[55] C. Schmitt, K. H. Schmidt, and A. Kelić-Heil, Phys. Rev. C **90**, 064605 (2014).
[56] B. L. Tracy *et al.*, Phys. Rev. C **5**, 222 (1972).
[57] A. Olmi and S. Piantelli, Eur. Phys. J. A **51**, 154 (2015).
[58] M. Wang *et al.*, Chin. Phys. C **36**, 1603 (2012).
[59] P. Möller *et al.*, At. Data Nucl. Data Tables **59**, 185 (1995).
[60] J. Benlliure *et al.*, Eur. Phys. J. A **2**, 193 (1998).
[61] O. B. Tarasov and D. Bazin, Nucl. Instrum. Methods B **266**, 4657 (2008).
[62] T. Rauscher, F. K. Thielemann, and K. L. Kratz, Phys. Rev. C **56**, 1613 (1997).
[63] S. Goriely, S. Hilaire, and A. J. Koning, Phys. Rev. C **78**, 064307 (2008).